PHYSICAL MECHANISMS FOR TRANSFER OF HEAT, MASS, AND MOMENTUM IN A SHORT LOW-TEMPERATURE HEAT PIPE. I. HYDRODYNAMICS OF VAPOR FLOW

P. I. Bystrov, A. I. Ivlyutin, V. N. Kharchenko, and A. N. Shul'ts

UDC 536.248.2

The authors present results of an experimental investigation of vapor flow hydrodynamics under positive pressure gradient conditions leading to boundary layer separation and the occurrence of a reverse vortex flow region of vapor in the condensation zone of a planar heat pipe. The influence of a noncondensible gas on heat and mass transfer and the configuration of the vapor gas front is examined.

A characteristic special feature of short heat pipes is inertia effects in the vapor, leading to displacement of the "wet" point to the start of the condensation zone. Friction in the vapor and in the liquid opposes this effect and displaces the wet point in contrary fashion to the end of the condensation zone. As a result the position of the wet point determines the maximum available heat transfer under conditions where the capillary head equals the total pressure loss along the vapor—liquid channel between the dry and the wet points. A positive pressure gradient due to inertia effects in the vapor flow can lead to boundary layer separation and formation of an S-shaped velocity profile characteristic of separated flows. Here the generation of reverse vortex flow increases the pressure loss in the vapor flow, changes the position of the wet point, and may limit the maximum available heat transfer.

The well-known models of hydrodynamics of vapor flow [1] are based on the idea that a velocity profile, symmetric relative to the heat pipe axis, parabolic for $Re_r \ll 1$ or cosine-shaped for $Re_r \gg 1$, is set up in the evaporator. However, this can occur only in a relatively long heat pipe, $l_c/l_e \gg 1$, where, as a rule, the velocity profile has a negative pressure gradient and correspondingly unseparated vapor flow in the condenser. These models do not account for the occurrence of asymmetry of the velocity profile in the evaporator, and the influence of its rearrangement on heat and mass transfer in the heat pipe condenser.

In addition, the generation of noncondensible gas resulting from thermochemical breakdown of the heat transfer agent, as well as special injection of noncondensible gas for control of heat pipe startup regimes, leads to the appearance of a vapor—gas front configuration, which appreciably affects the startup and the limiting heat pipe characteristics. A knowledge of the special features of interaction of the vapor and gas phases, their distribution over the heat pipe volume, the flow structure and the regimes for different heat flux is important for construction of controlled heat pipes capable of transferring variable heat loads of high specific power q. A considerable number of papers [1-9] have studied processes of heat and mass transfer in heat pipes with noncondensible gas. However, the results available as yet are not enough to develop reliable methods of planning and designing heat pipes of this type.

In theoretical investigations of heat pipes with noncondensible gas [2-5] it is usual to examine a diffusion exchange mechanism between the vapor stream and the gas, which promotes the formation of a planar vapor—gas front configuration perpendicular to the heat pipe axis. Similar conditions can be achieved in small-diameter long heat pipes during transfer of small heat fluxes. It was shown in [6, 7] that with increase of $q > 10^4$ W/m^2 the dominant heat transfer process becomes forced convection. The intense transfer along the condensation zone leads to the formation of an unstable vapor—gas front configuration, subject to the influence of hydrodynamic vapor flow fluctuations.

The experimental investigations of [8, 9] revealed a more complex picture of heat and mass transfer in comparison with the flow model presently assumed in the heat pipe. This was primarily due to the existence of different hydrodynamic regimes along the heat pipe and the variation of the vapor flow structure due to the appearance of liquid drops thrown out from the wick structure and to volume condensation processes.

Moscow Institute of Forest Technology. Translated from Inzhenerno-Fizicheskii Zhurnal, Vol. 60, No. 1, pp. 5-12, January, 1991. Original article submitted January 24, 1990.

0022-0841/91/6001-0001$12.50

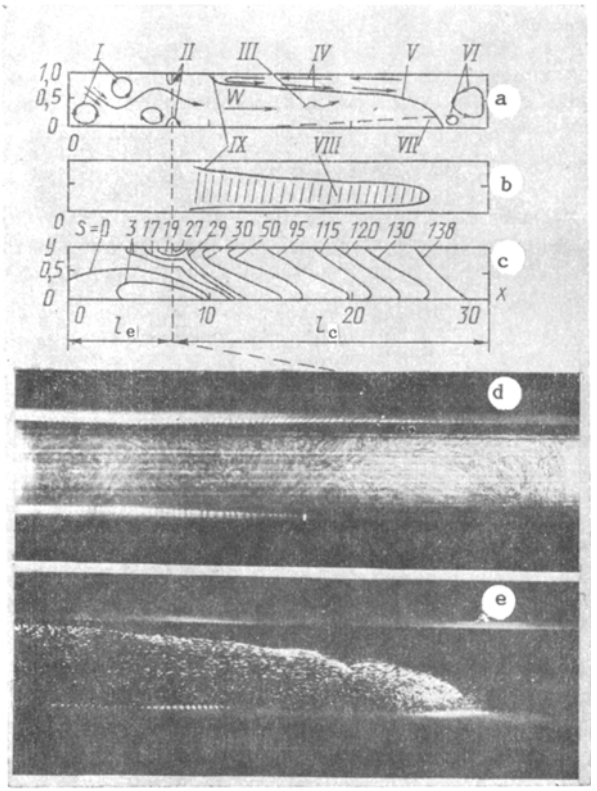

Fig. 1. Visualization of optical nonuniformities; heat transfer agent is acetone, Q = 230 W, $P_{ncg} = 1.2 \cdot 10^4$ Pa: a) flow visualization by the knife-edge method with light source LGN404A; I) vortex structure in the evaporator zone; II) vortices rotating in the blowing-suction direction; III) main flow in which particles move in small-scale helical trajectories oriented along the flow, longitudinal vortices; IV) region of reverse vortex flow; V) interface of opposing streams, vapor—gas front configuration; VI) vortices closing the flow; VII) region of drop motion along falling trajectories; b) shadowgraph flow picture VIII) region of high optical density, main vapor flow; IX) region of boundary layer separation; c) flow interferogram, tuning of Mach—Zender interferometer to a band of infinite width, 0-138 is the optical difference of S; d) flow photograph of acetone vapor at the evaporator exit, a dotted line showing the evaporator exit section, the exposure time being τ = 0.5 sec, and the knife-edge thickness is $\Delta = 3 \cdot 10^{-3}$ m; e) flow photograph of acetone vapor in the condenser, exposure time τ = 1/30 sec.

The aim of the present work is to investigate the hydrodynamics of vapor flow in the conditions: a) boundary layer separation and the occurrence of a region of reverse vortex flow; b) draining of the noncondensible component during homogeneous or homogeneous-heterogeneous volume condensation in the vapor flow.

Experimental Equipment and Investigative Technique. The investigation was carried out in a planar heat pipe [6, 8] which had a rectangular body with lateral transparent walls of dimensions: total length 595 mm, length of evaporation zone 145 mm, condensation zone 450 mm, channel height 19 mm; the wick was a composite stainless steel mesh and cloth felt No. 120/670 GOST 3187-65, and the gap under the wick screen was 0.3 mm. Heat was supplied to the evaporator by forced pumping of heat transfer agent through the intersleeve gap, and was removed in the condenser by pumping of cooling agent. The heat pipe was equipped with a system of side wall heating to maintain adiabatic conditions there and avoid the appearance of a condensation film which would obstruct optical visualization. With the measurement system one could record: the vapor temperature distribution in transverse sections of the heat pipe, the heat balance in the evaporation and condensation zones, the distribution of optical nonuniformities using a

Mach—Zender interferometer and a schlieren system; and visualize the flow with the aid of a knife edge. The density, pressure and humidity of the vapor at transverse sections of the heat pipe were determined from results of reducing interferograms of boundary layer density. To calibrate the interferograms we used the experimentally measured temperature distributions at transverse sections of the heat pipe. It was assumed here that the schlieren path consisted of a mixture of saturated and unsaturated vapor, and drops of condensed liquid for which the ratio $2\pi R_c/\lambda \gg 1$ holds, and that scattering of light does not contribute to the schlieren path. The added humidity of the vapor due to the liquid phase content was determined in the form of a correction $\Delta\varepsilon$ to the vapor humidity ε found from the interferograms. The correction $\Delta\varepsilon$ was found by determining the number and size of liquid drops in the vapor stream from photographs.

It is known [10] that the variation of the refractive index depends on

$$dn = \left(\frac{\partial n}{\partial T}\right)_c dT + \left(\frac{\partial n}{\partial C}\right)_T dC, \tag{1}$$

where C is the local density.

For phase transitions one can consider that:

$$\left(\frac{\partial n}{\partial T}\right)_c dT \ll \left(\frac{\partial n}{\partial C}\right)_T dC. \tag{2}$$

Convective mass transfer with suction or blowing can be described by [11]:

$$m = -D_c \frac{d\rho}{dy} \approx W \frac{\delta}{2} \frac{d\rho}{dy}, \tag{3}$$

where W is the bulk flow velocity, determined from integral relations according to the chosen heat pipe volume. Then for sections for which there is no noncondensible gas, the convective heat transfer with suction or blowing is determined from the formula:

$$q = m\varkappa = -\varkappa D_c \frac{d\rho}{dy}, \tag{4}$$

where ρ is identically equal to C.

The monochromatic light of wavelength λ, passing through the plane—parallel nonuniform low of thickness L, causes displacement of the interference bands $S(x, y)$, described by the equation of the ideal Mach—Zender interferometer [10]

$$S(x, y) = L/\lambda [n(x, y) - n_e]. \tag{5}$$

For heat transfer agent vapor whose refractive index is close to 1 the ratio between the refractive index $n(x, y)$ and the density can be written in the form of the Gladstone—Dale equation [10]

$$\frac{2[n(x, y) - 1]}{3\rho(x, y)} = \bar{r} = \text{const}. \tag{6}$$

Then from Eqs. (5) and (6) we obtain the required expression

$$\frac{\rho(x, y)}{\rho_e} = 1 + \frac{\lambda S(x, y)}{L(n_e - 1)}. \tag{7}$$

At the start of the evaporation zone, where the vapor flow is practically stationary, $W = 0$, and the vapor state corresponds to the saturation parameters, and the gradients of temperature and pressure are close to zero. The refractive index corresponding to these parameters was determined from the known saturation temperature of the vapor flow in this zone of the heat pipe:

$$\frac{n_e - 1}{n_0 - 1} = \frac{\rho_e}{\rho_0}. \tag{8}$$

Here for acetone $n_0 = 1.001096$ at $T_0 = 273$ K, $\rho_0 = 2.59$, and $\rho_e = 2.42$ kg/m^3.

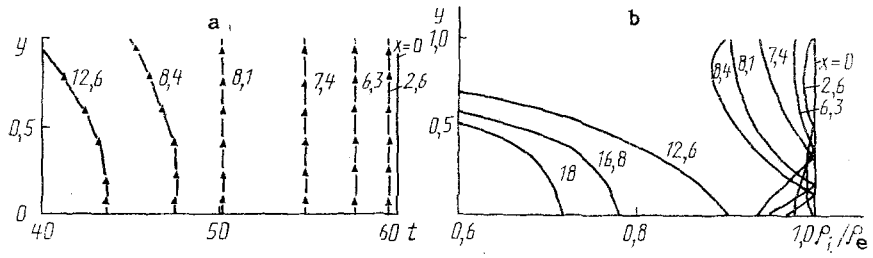

Fig. 2. Experimental determination of the parameters of moist vapor in transverse sections of the heat pipe: a) temperature, from the thermocouple measurements, °C; b) relative density ρ_i/ρ_e from results of smoothing the interferograms, Eq. (7) (regime of Fig. 1).

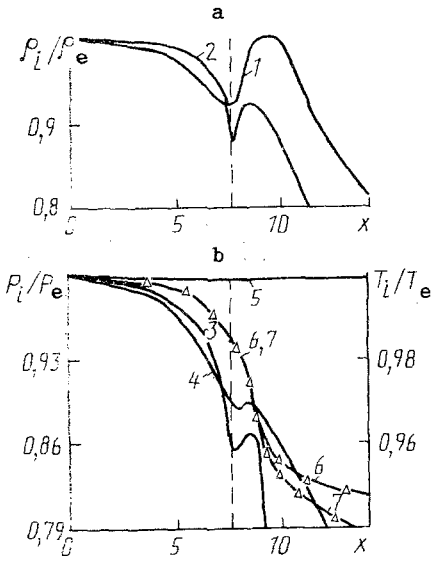

Fig. 3

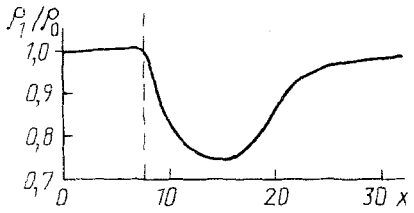

Fig. 4

Fig. 3. Distribution of parameters of the moist vapor along the upper surface $y = 1$ and the lower surface $y = 0$ of the heat pipe wick: a) relative density ρ_i/ρ_e, smoothing of the interferogram, Eq. (7), 1) $y = 0$, 2) $y = 1$; b) relative pressure P_i/P_e, smoothing of the interferogram using Eq. (9), 3) $y = 1$, 4) $y = 0$; 5) P_i/P_e from calculation using Eqs. (11) and (12); 6, 7) relative temperature T_i/T_e, 6) $y = 0$, 7) $y = 1$.

Fig. 4. Change in relative density ρ_1/ρ_0 along the lower surface y = 0 and upper surface y = 1 of the heat pipe wick (smoothing of the interferogram according to Eq. (7)).

Subsequent processing of the interferograms was done in the ideal gas model approximation using the formula

$$\frac{P(x,\ y)}{P_e} = \frac{\rho(x,\ y)}{\rho_e}\,\frac{T(x,\ y)}{T_e} = \frac{T(x,\ y)}{T_e}\left[1 + \frac{\lambda S(x,\ y)}{L(n_e - 1)}\right], \tag{9}$$

where $\lambda = 0.6328\ \mu$, $L = 0.145$ m.

In final form the heat flux with suction and blowing in the heat pipe was found from the expressions

$$q_{0,1} = \varkappa D_c \frac{\lambda \rho_e}{L_e(n_e - 1)}\left[\frac{dS(x,\ y)}{dy}\right]_{y=0,1}. \tag{10}$$

The pressure drop in the vapor due to acceleration and friction was evaluated from the formulas [1]

$$\Delta P_e = \frac{8\pi^2 Q^2}{d_{eq}^4 \varkappa^2 \rho_v}\left(\frac{\pi^2}{4} + \frac{f_f l_e}{d_{eq}}\right), \tag{11}$$

$$f_f = 2\pi/\mathrm{Re} + 0{,}03/\mathrm{Re}^{0,2}. \tag{12}$$

Analysis of the Experiments. As heat transfer agent we used water, and alcohol and acetone. The most suitable for flow visualization was acetone. With the small heat of phase transition and the high refractive index of acetone vapor we could obtain significant gradients of optical nonuniformity for low heat flux Q = 100-300 W.

To investigate the range of heat flux it was established that along the heat pipe there are differences of intensity of the fluctuating motion and of the content of condensed phase of the vapor flow regimes (Fig. 1). In the blowing region studied $\mathrm{Re}_r \leq 12$ the evaporation zone is characterized by complete development of vortex flow. This is confirmed by tracks of particles thrown out under boiling (Fig. 1a), and by the shadowgraph pictures (Fig. 1b). The large-scale transverse eddies with a specific periodicity originate at the start of the evaporation zone and move downstream. The dimensions of the vortices carried downstream were one-third the height of the channel, and their velocity of displacement increased with increasing heat flux. Analysis of the flow visualization picture showed that the existence of vortex flow in the evaporation zone is due to hydrodynamic instability of plane—parallel flow with blowing [12]. This kind of flow regime has a considerable influence on the dynamics of the flows in the condensation zone, leads to the occurrence of turbulent fluctuations in the condenser, and to propagation of these downstream even in the vapor—gas front configuration.

At the interface of the evaporation and condensation zones there arise also two unsteady transverse vortices, rotating oppositely in the direction of mass blowing and suction (Fig. 1a). The flow core, subject to hydrodynamic compression on the vortex side, expands into the condensation zone, filing the whole section of the heat pipe channel. Here the flow becomes laminar, and there is appreciable straightening of the tracks of particles (Fig. 1a). It was established from photographs with long exposure time that the particle trajectories are small scale ~$\delta/20$ helical lines oriented along the flow. This reflects rearrangement of the vortex motion, comprising degeneration of the transverse vortices and the establishment of flow formed by a set of longitudinal vortices. This region was found at the start of the condenser, and its dimensions did not exceed 2δ. Just here x = 8.4, Q = 235 W there was maximum heat removal from the vapor flow and a sharp increase of the number of liquid particles.

The fracture of the interference lines in a thin layer near the heat transfer surface of the evaporator and the condenser indicates a variation of the intensity of radial and axial transfer of mass and momentum downstream, evaluated from the ratio of local Reynolds numbers $\mathrm{Re}_r/\mathrm{Re}_0$ in the chosen heat pipe element [1].

It follows from analysis of the gradients of the optical nonuniformities that the computed pressure drops in the evaporator zone (Eq. (9)) do not agree with the distribution of pressures obtained from smoothing the interferogram in the one-component ideal gas model approximation, Eqs. (11) and (12). For example, for the regime shown in Fig. 1 the computed pressure drop in the evaporator zone $\Delta P_e < 1$ Pa, while one interference band is associated with ΔP = 511 Pa. This indicates that in the vapor flow there are components with refractive indices larger than in the original material, e.g., the dimer acetone molecule. The concentration of dimer molecules was estimated according to the two-component ideal gas model, consisting preferentially of the monomer—dimer mixture, from the formulas $\rho = P/R_e T(1 + \alpha)$, $N_e = (1 - \alpha)/(1 + \alpha)$. For the experimental interferogram to agree with the computed value of pressure at the evaporator outlet the molar concentration of dimer at this section should be N_e = 0.084. Subsequent analysis of the hydrodynamics of the vapor flow was performed, allowing for possible formation of dimer molecules of acetone.

In the heat flux range studied two-phase flow arose in operating bodies with relatively low heat phase transition (ethyl alcohol, acetone). Calculation showed that the appearance of drops in the condensation zone due to interaction of the opposing streams of vapor and heat transfer agent in the wick was impossible, since the Weber number, which characterizes this process, is $\mathrm{We} = \rho W^2 R_{ef}/\sigma < 1$. The vapor speed W and the Reynolds number were determined from relations for the bulk magnitudes. The size of a drop carried freely by the flow was evaluated from the expression [13]

(13)

where the "wander" speed was assumed to equal the vapor speed [14], and the quantity ξ was 0.4 for $10^3 < Re_0 < 2 \cdot 10^5$, from [15].

Drops which visualized the boundaries of the reverse-vortex flow regions IV and VI (see Fig. 1a) satisfied the relation $R < R_c$ from Eq. (13).

When a small amount of noncondensible gas is present in the working volume of the heat pipe (e.g., air with initial partial pressure $P_{ncg} = 1.2 \cdot 10^4$ Pa prior to startup of the heat pipe), the flow character described did not change in principle, but the interface became more pronounced because of the increasing density of liquid particles. With increase of initial pressure of noncondensible gas the layering of the flow increased and the boundary of the gas—vapor front configuration appeared. In the gas—vapor front region the drops increase in size, moving along the gas—vapor front configuration, and reached a specific size, penetrating into the volume of the main flow and into region VII, where they moved along the falling trajectory to the lower surface of the condenser wick.

Depending on the ratio of the molecular weights of noncondensible gas and heat transfer agent, a different gas—vapor front configuration was established. For $\mu_{hta}/\mu_{ncg} < 1$ (e.g., water—air) the reverse-vortex flow region was localized at the bottom. Then the direction of convective motion in this region was changed.

Deformation of the density profiles began at the start of the evaporation zone, and the flow core was displaced to the lower surface of the heat pipe (sections x = 7.4; 8.1; 8.4, Fig. 2). It follows from analysis of the interferograms that the region of positive density gradient (see Fig. 1) is considerably larger than the region on the lower surface. At the bottom this region was localized in a thin layer of about ~1 mm, and at the top it occupied one third of the channel. The pressure distribution in the evaporator was established according to the reverse-vortex flow arising in the condensation zone. In established form the hydrodynamic field of vapor flow is characterized as follows: in the evaporator by rotation of the axis of the main flow towards the lower surface of the heat pipe; in the condenser by the generation of an S-shaped velocity profile in the entire flow region.

As can be seen from Fig. 3a (curves 1, 2) the densities at the lower and upper surfaces of the condenser differ considerably. Such a difference cannot be explained by the difference of temperatures (Fig. 3b, curves 6, 7), according to which it is $\rho_1/\rho_0 = 0.98$, using the one-component ideal gas model. For $\rho_1/\rho_0 < 0.98$ the density difference is due to the change of flow composition due to the presence of the noncondensible gas (Fig. 4). Hence it follow that the noncondensible gas, deflected into the reverse-vortex flow region, considerably changes the composition of vapor flow over the heat pipe section. The thermal resistance of both condenser plates increases due to lowering of the partial pressure of vapor as one draws near to the heat transfer surface of the condensation zone. The propagation of noncondensible gas across the main flow can occur due to diffusion processes, since there is no convection in this direction. The slowly flowing diffusion processes cannot keep pace with convective mass transfer in the reverse vortex flow region, and therefore there is considerably greater thermal resistance at the top surface of the condenser, than at the lower surface.

Conclusions. It was observed experimentally that:

1. In the heat flux range Q = 100-300 W in the evaporation zone a vortex flow regime was created, consisting of a system of transverse vortices moving downstream, with a scale of ~$\delta/3$, smoothing out the main vapor flow. At the evaporator exit, in the region where the mass flow action changes sign, the transverse vortices break down and are transformed into small-scale longitudinal vortices which keep their transverse dimensions of $\delta/20$ as they propagate further in the condenser. The region of rearrangement of the vortex flow coincides with that of maximum heat removal.

2. Inertia effects in the vapor can lead to a positive pressure gradient, separation of the boundary layer, and the formation of an S-shaped velocity profile in the condenser. Deformation of the profiles of density and velocity begins 8-10 calibers ahead of the separation point and leads to a considerable asymmetry.

3. Noncondensible gas, deflected into the reverse-vortex flow region, considerably increases the thermal resistance. This process promotes stratification of the flow of vapor and noncondensible gas. To avoid the occurrence of regions of reverse vortex flow and improve the heat and mass transfer characteristics in this regard it is desirable to shape the vapor channel of the condenser according to the condition $dP/dx = 0$ by contracting the channel or setting up a centerbody.

4. The position and configuration of a vapor—gas front are determined by the level of transmitted heat power and the ratio of the molecular weights of the heat transfer agent and the noncondensible gas.

NOTATION

n index of refraction; q, heat flux, W/m^2; R_d, drop radius, m; D_c, convective diffusion coefficient, m^2/sec; $\bar{r}$, specific refractive power, m^3/kg; $\varkappa$, specific heat of phase transition, J/kg; $S(x, y)$, optical path difference; $x = x_i/\delta$, relative length of the heat pipe; $y = y_i/\delta$, relative height of the heat pipe vapor channel; Q, thermal power, W; N, molar density of the molecules; μ, molecular weight, kg/kmole. Subscripts: p, partial; a, axial; c, condenser; e, evaporator; d, dimerification of molecules; l, liquid; s, saturation; eff, effective; hta, heat transfer agent.

LITERATURE CITED

1. M. N. Ivanovskii, V. P. Sorokin, and I. V. Yagodin, Physical Fundamentals of Heat Pipes [in Russian], Moscow (1978).
2. E. K. Levi, J. Eng. Ind., **80**, 547-551 (1968).
3. P. Zimmerman, Proc. IEEE Thermionic Conversion Specialist Conf., 567-570 (1970).
4. A. R. Rokhani and S. L. Dyan, Trans. ASME, Ser. C, Teploper., Vol. 95, No. 3, 92-98 (1973).
5. Van Owen and J. K. Khogendorn, Raket. Tekh. Kosmon., **17**, No. 11, 122-132 (1979).
6. A. N. Shul'ts, Heat Transfer in Technological Processes [in Russian], No. 138, Moscow (1981), pp. 62-65.
7. V. V. Galaktionov, A. A. Parfent'eva, V. D. Portnov, and V. Ya. Sasin, Inzh.-Fiz. Zh., **42**, No. 3, 387-392 (1982).
8. A. I. Ivlyutin, V. N. Motorin, and V. N. Charchenko, Proc. All-Union Conf. Heat/Mass Transfer, Minsk, Vol. IV, Pt. 1, 79-84 (1984).
9. V. D. Portnov and A. A. Parfent'eva, Proc. All-Union Conf. Heat/Mass Transfer, Minsk, Vol. IV, Pt. 1, 129-133 (1984).
10. V. Khauf and Ts. Grigul, Optical Methods in Heat Transfer [in Russian], Moscow (1973).
11. A. A. Gukhman, Use of Similarity Theory to Investigate Heat and Mass Transfer Processes [in Russian], Moscow (1974).
12. A. L. Ermakov, V. M. Eroshenko, A. A. Klimov, et al., Izv. Akad. Nauk SSSR, Mekh. Zhidk. Gaza, No. 6, 114-123 (1972).
13. S. S. Kutateladze and M. A. Styrikovich, Hydrodynamics of Gas—Liquid Systems [in Russian], Moscow (1976).
14. M. A. Styrikovich, O. I. Martynova, and Z. L. Miropol'skii, Processes of Generating Steam in Power Stations [in Russian], Moscow (1969).
15. Technical Encyclopedia, Vol. 8 [in Russian], Moscow (1932).